A Review of PDE Based Local Inpainting Methods

A Review of PDE Based Local Inpainting Methods

Ahmed K. Al-Jaberi[1*], and Ehsan M. Hameed[2]

[1] Department of Mathematics, College of Education for Pure Science, University of Basrah, Basrah, Iraq.
[2] Department of Mathematics, College of Computer Science and Mathematics, University of Thi-Qar, Thi-Qar, Iraq.

E-mail: ahmed.shanan@uobasrah.edu.iq

Abstract. Image inpainting is the process of recovering the damage areas in the images in an undetectable way, it is considered the important one of the subjects in image processing. There are many applications of image inpainting include the restoration of damaged images, paintings, and movies, to the removal of selected objects, such as text, lines, subtitles, publicity, and stamps. The main objective of inpainting is to reconstruct the missing region in such a way that the observer does not come to know that the image has been manipulated. Inpainting methods can be categorized into global and local methods, the global methods are applied to reconstruct the damaged areas in the image based on the information in the data of images that have the same content. While the local methods are used to reconstruct the missing regions based on the information in the rest parts of the image. There are several local methods proposed for image inpainting such as PDE-based inpainting (PDE-BI), exemplar-based inpainting (EBI), hybrid, and texture synthesis methods. In this paper, a review of different PDE and variational methods used for image inpainting is provided. Different PDE-BI methods like 2nd- and high-order of variational and PDE methods are discussed with its pros and cons.

1. Introduction

Inpainting is the process of restoring the lost or deteriorated areas in images/movies based on the information in the rest areas of images. The deteriorated images modify in a way that is non-detectable for an observer by using inpainting methods. These methods have found widespread use in many applications such as reconstructing old images, movies, and painting, super-resolution, image coding, image compressions, transmission, removal of occlusions, such as object, text, or scratch in images, etc. A several local methods are proposed for image inpainting and each one of these methods has a lot of studies in the literature, such as PDE-BI [1], [2], [3], [4], [5], [6], [7], exemplar-based inpainting (EBI) [8], [9], [10], [11], hybrid [12], [13], [14], and texture synthesis methods [15], [16].

The basic idea of PDE-BI methods in the reconstruction of destroyed regions in images by propagating the information from the boundary of the destroyed area into it, where these methods propagate the

information pixel by pixel in the destroyed regions in the image. The inpainting task is introduced and clarified in Figure 1, where $\boldsymbol{f}$ is a given image, $\boldsymbol{\Omega}$ is an image domain, and the damaged domain $\boldsymbol{D} \subset \boldsymbol{\Omega}$ in damaged image $\boldsymbol{u}$. The damaged domain represents a set of pixels, which are often indicated as objects, texts, scratches, and holes.

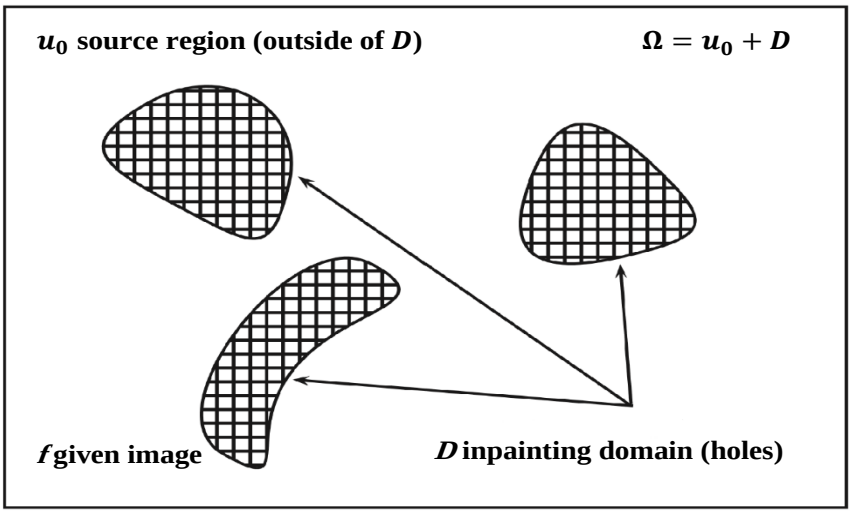

Figure 1. The inpainting task.

Mathematically, the inpainting methods are categorized as variational (Energy) methods and direct non-variational (PDE-BI) methods. Variational methods apply to the damaged image as a functional minimizer (image). Then, the Euler-Lagrange equation is used on the minimization of functional to produce a PDE. While PDE-BI methods are directly applied to images by the use of mathematical approximation theory in bounded of the rich and well-established of 2-variables functions. PDE-BI models are well covered in the literature by researchers. Some other PDE-BI models for image gapes reconstruction such as Heat diffusion [17], Harmonic [18], Navier-stokes [19], and Transport [1], will be presented in Section 4.

The art restoration workers introduced the inpainting task in [20] and [21]. Bertalmio et al. firstly introduced a discrete 3rd-order non-linear PDE aimed to mime the reconstruction work of museum artists in [1]. The destroyed region is automatically recovered by using the isophote operator (i.e. connecting the lines to the boundaries of it). The pioneering works of variational-based inpainting methods, Bertalmio (Transport) [1], Mumford-Shah [2], Total Variation (TV) [22], Curvature of Driven Diffusion (CDD) [23], High order Total Variation [24], Mumford-Shah-Euler [25], Chan-Hilliard [26], Isotropic Diffusion [17], Harmonic-Extension [18], Euler-Elastica and curvature [27] and Navier-stokes [19] in the last two decades, will review in section 4.

This paper is an overview of several PDE- and variational-based inpainting methods and describes some of the commonly used methods to solve complex problems with image inpainting methods. The rest of the paper is organized as follows. Section 2 describes the various ways of classification of inpainting methods. Section. 3 introduces PDE-BI methods. Variational-based inpainting methods are clarified in Section 4. The comparison of these methods presents in Section 5. Finally, conclusions and future work will display in section 6.

2. Classifications of Local Inpainting Methods

There are several classifications of local inpainting methods in terms of size of damaged areas, the quantity of texture in the surrounding areas of damaged areas, the process of information propagation, type of underpinning theories and its applications, and based on the operation domain.

So, inpainting methods can be categorized in terms of the process of information propagation in the missing regions. These techniques are divided into texture synthesis and/or EBI methods which spread the information block by block from the surrounding areas to the missing region [8], [9], [10], [11], [15], [16] and PDE-BI methods which propagate the information pixel by pixel from the rest of the image to the damaged area [24], [25], [28], [29].

In another way, inpainting methods can be categorized in terms of the size of damaged areas in the image. These methods are split into texture synthesis, EBI, and/or hybrid methods which utilized to restore large missing regions in the images [8], [9], [12], [13], [14], [15], [16] and PDE-BI methods which used to recover small damaged areas in the images (i.e. scribbles, texts, and dates) [18], [30], [31].

Also, inpainting methods can be categorized according to the quantity of texture in the surrounding areas of the damaged region in the image. These methods divided into texture synthesis and/ or hybrid methods which used to reconstruct high-texture areas in the images [12], [13], [15], [16] and PDE-BI methods which utilized to recover low-texture missing regions in the images [32], [18], [24].

Finally, inpainting methods can be classified in terms of operation domain into Fourier and wavelet domains. It is worth noting, several inpainting methods have been introduced to reconstruct the missing density data and/or the missing transformed data [33], [34].

3. Variational-BI Methods

The variational methods are best clarified as an inverse problem. Image inpainting aims to reconstruct an original image $\boldsymbol{u}$ from the damaged image $\boldsymbol{f}$. Mathematically, let $\Omega \subset \boldsymbol{R^2}$ be an open and bounded set, and $\boldsymbol{D} \subset \Omega$ is a destroyed domain. So the solution to this inverse problem, we should solve $\boldsymbol{T_u = f}$, where $\boldsymbol{T}$ is an operator that describes the process by recovering the damaged image $\boldsymbol{f}$. The formula 3.1 defines a minimization problem which describes a general variational method in image inpainting.

$$\min_{\boldsymbol{u}\in\Omega} \|\boldsymbol{T_u - f}\|_{\Omega}^{2} \qquad (\mathbf{3.1})$$

The solutions of (3.1) is an ill-posed when the operator $\boldsymbol{T}$ possesses an unbounded inverse. To defeat this problem, a regularization method is applied by adding terms to represent the convexness of disoccluded shapes, straightness of the edges, and smoothness-related properties. For example, a TV model [22] is applied to appear the image smoothness. The behavior of the model (3.1) will change to a regularised and well-posed model after applying the regularization method on it, as following:

$$\boldsymbol{E(u)} = \min_{\boldsymbol{u}\in\Omega}\{\boldsymbol{\alpha \mathcal{R}(x, u, Du, \dots, D^k u) + \lambda_0 \|T_u - f\|_{\Omega}^{2}}\}, \qquad (\mathbf{3.2})$$

$$\boldsymbol{\lambda(x)} = \begin{cases} \boldsymbol{\lambda_0} & \boldsymbol{if\ \ x \in \Omega \backslash D} \\ \mathbf{0} & \boldsymbol{if\ \ x \in D,} \end{cases}$$

where $\boldsymbol{\alpha > 0}$ and $\boldsymbol{\lambda_0}$ are regularization parameters. The term $\boldsymbol{\mathcal{R}(\mathbf{u})}$ is a regularizing term (i.e. is data term) whereas $\|\boldsymbol{T_u - f}\|_{\Omega}^{2}$ is known as the fidelity term. The formula (3.2) plays an essential role in recovering the damaged image [18], such as diffusion and/or transport models.

The Euler-Lagrange equation applies to find the minimization of $\boldsymbol{u}$, i.e. finding the derivative of the functional operator $\boldsymbol{E}$ in (3.2). For applying the Euler-Lagrange equation of minimizer $\boldsymbol{u}$, the Fréchet derivative uses on $\boldsymbol{E}$, and should be zero, this reads

$$-\boldsymbol{\nabla\mathcal{R}}\left(\boldsymbol{x},\boldsymbol{u},\boldsymbol{Du},\dots,\boldsymbol{D^k u}\right)+\boldsymbol{\lambda_0}(\boldsymbol{T_u}-\boldsymbol{f})=\boldsymbol{0},\ \ \boldsymbol{in\ \Omega} \tag{3.3}$$

The steepest descent or gradient flow method applied on (3.3) to get the dynamic version (3.4). This is a PDE with certain boundary conditions on $\boldsymbol{\partial\Omega}$, where $\boldsymbol{\nabla\mathcal{R}}$ represents the Fréchet derivative of $\boldsymbol{\mathcal{R}}$. More precisely, a minimizer u of (3.2) is embedded in an evolution process, represented by $\boldsymbol{u}(\cdot,\boldsymbol{t})$. When $\boldsymbol{t}=\boldsymbol{0}$, then $\boldsymbol{u}(\cdot,\boldsymbol{t}=\boldsymbol{0})=\boldsymbol{f}$, this means it is the original image. After that, this image converted through an iterative method, which introduced as

$$\boldsymbol{\partial_t u}=-\boldsymbol{\nabla\mathcal{R}}\left(\boldsymbol{x},\boldsymbol{u},\boldsymbol{Du},\dots,\boldsymbol{D^k u}\right)+\boldsymbol{\lambda_0}(\boldsymbol{T_u}-\boldsymbol{f}),\ \ \boldsymbol{in\ \Omega},\qquad \textbf{and}\qquad \boldsymbol{\partial_n u}=\boldsymbol{0}\quad \boldsymbol{on\ \partial\Omega}, \tag{3.4}$$

The formula (3.4) is iteratively solved till one is near sufficient to a minimizer of $\boldsymbol{E}$. The numerical solution of a PDE (3.4) over the bounded variation space of functions $\boldsymbol{BV}(\boldsymbol{\Omega})$ (i.e. digital images), this solution succeeded in noise removal or destroyed- region reconstruction, (see [17]). Variational methods are focused on the continuity of the geometrical structure of an image by using the isophotes operator. Variational methods are well at recovering the small-narrow regions in the images. Also, these methods cannot be used for recovering missing texture regions. Next, a review of some different variational-BI methods will introduce.

3.1.Total Variation Model (Anisotropic Diffusion)

Inspired by Bertalmio [1], the TV model has been introduced by Shen and Chan in [22]. The Euler-Lagrange equation and anisotropic diffusion have been used in this model. The anisotropic model was originally introduced for noise removal from an image with edges preservation in the image. This model was introduced based on the spread stationary with the size of the image gradient, to decrease the quantity of overlap that happens close to the edges [22]. The anisotropic equation is a non-linear 2nd-order PDE, which treats the faults that appear through applying the isotropic and harmonic equations. Two ways have been used to introduce this model:

$$\begin{cases} \boldsymbol{\partial_t u}=\boldsymbol{div}\left(\frac{\boldsymbol{\nabla u}}{|\boldsymbol{\nabla u}|}\right),\ \boldsymbol{t}\geq\boldsymbol{0}, \\ \boldsymbol{u}(\boldsymbol{0},\boldsymbol{x},\boldsymbol{y})=\boldsymbol{u_0}(\boldsymbol{x},\boldsymbol{y}),\ \ \boldsymbol{0}\leq\boldsymbol{t}\leq\boldsymbol{T}. \end{cases} \tag{3.5}$$

The equation (3.5) with the Neumann boundary condition is applied to recover the small damaged area in the image. Also, the anisotropic equation can be introduced as minimization of the TV model:

$$\underset{\boldsymbol{u}\in\boldsymbol{L^1(\Omega)}}{\boldsymbol{min}}\left\{\int_{\boldsymbol{D}}|\boldsymbol{\nabla u}|\ \boldsymbol{d\Omega}\ \ \textbf{such that}\ \boldsymbol{u}=\boldsymbol{f}\ \boldsymbol{in\ \Omega\backslash D}\right\} \tag{3.6}$$

The Euler Lagrange equation has used on functional minimization (3.6) then the gradient descent method has applied to it, as follows:

$$\boldsymbol{\partial_t u}=\boldsymbol{div}\left(\frac{\boldsymbol{\nabla u}}{|\boldsymbol{\nabla u}|}\right) \tag{3.7}$$

For image denoising [7], the fidelity term has been added to the anisotropic model (3.6), leads to

$$\underset{\boldsymbol{u}\in\boldsymbol{L^1(\Omega)}}{\boldsymbol{min}}\ \boldsymbol{F}(\boldsymbol{u})=\int\int_{\boldsymbol{\Omega}}\left(|\boldsymbol{\nabla u}|+\frac{\boldsymbol{\lambda}}{\boldsymbol{2}}(\boldsymbol{u}-\boldsymbol{f})^{\boldsymbol{2}}\right)\boldsymbol{dxdy} \tag{3.8}$$

The Euler-Lagrange equation is applied on (3.8), after that the gradient descent method is used, leads to

$$\partial_t u = div\left(\frac{\nabla u}{|\nabla u|}\right) + \lambda(u - f) \qquad (3.9)$$

The numerical method is applied to equation (3.9) with Neumann boundary condition when u define in L2. While this numerical method is implemented to solve model (3.9) with Dirichlet boundary condition when u define in L1. Also, the TV model has been applied in the wavelet domain which reconstructs the structure in the image [33]. Finally, this model performs well for recovering small damaged areas and noise removal. However, this model is failed to connect broken edges and recover textured areas.

3.2.Fourth-Order Total Variation Model

The 4th-order TV model addresses the flaws of the 2nd- order TV model. This model resembles a generalization of the mCH model when defined on gray images [24]. The formula of this model is:

$$\partial_t u = -\triangle\left(div\left(\frac{\nabla u}{|\nabla u|}\right)\right) + \lambda(\vec{x})(f - u) \qquad (3.10)$$

The fitting term is a gradient flow of the energy defined in H^{-1} and L^2, respectively. The convexity splitting method is applied on (3.10), and then a time-stepping scheme will use to recover the destroyed areas in the image. This numerical solution of model (3.10) with two boundary conditions produces clear improved results, particularly on edges. Finally, the curvature preservation and the connectivity principle are realized over applying it for reconstructing the big destroyed areas.

3.3.Curvature of Driven Diffusion Model (CDD)

The CDD model has been proposed by Shen in [23] to improve the performance of the 2nd-order TV model for recovering the big areas and linking the lines/curvature across large distances. This model is a 3rd-order non-linear PDE method. The improvement is possibly due to this model is a 3rd-order non-linear PDE efficiency whilst TV methods are a 2nd-order (linear and non-linear) PDEs can only rebuild small regions [2], and difficulty reconstruct the edges and corners [36]. The formula of the CDD model is

$$\partial_t u = \nabla \cdot \left[\frac{g(|k|)}{|\nabla u|}\nabla u\right] \qquad (3.11)$$

Where $k = \nabla \cdot \left[\frac{\nabla u}{|\nabla u|}\right]$ which is the scalar curvature of isophote through pixel x. And g is the annihilator of large curvatures and stabilizer of small curvatures:

$$g(k) = k^p, \quad k > 0, p \geq 1.$$

The CDD model is used to reconstruct the damaged areas based on the curvature information of the isophotes. However, this model can only be used to recover the non-textured structure since the texture can struggle away.

3.4.Mumford-Shah Model (MSm)

The MSm was firstly introduced for image segmentation issues [37]. After that, this model was introduced for image restoration matters [25]. The formula of the minimization energy is

$$\boldsymbol{E[u,\Gamma] = \min_{u} F(u) = \frac{\lambda}{2}\int_{\Omega\setminus D}(u-f)^2 d\vec{x} + J[u,\Gamma].} \quad (3.12)$$

with

$$\boldsymbol{J[u,\Gamma] = \frac{\gamma}{2}\int_{\Omega\setminus\Gamma}|\nabla u|^2 d\vec{x} + \beta_0 \mathcal{H}^1(\Gamma).} \quad (3.13)$$

Where $\vec{x} = (x, y)$, γ and β_0 are non-negative constant parameters, $\mathcal{H}^1$ refers to 1-dim Hausdorff space which calculates the length of curves in the area, and Γ refers to the edges in an image. Where formula (3.12) proposed to reconstruct a destroyed area into its piecewise smooth area u in the H^1 space and its edge set Γ in 1-dim Hausdorff space $\mathcal{H}^1(\Gamma)$. After that, the Euler-Lagrange Equation is applied on (3.12), which produces a non-linear 2nd-order PDE. The Ambrosio-Tortorelli approximation method applies to numerically solve this model (3.12), for more information about numerical solution can be found in [38]. This model works well and fast for small regions, while produced blurred results for large damaged regions, and textured damaged regions.

3.5.Euler-Elastica and Curvature-Based Inpainting

Euler-Elastica and curvatures model proposed by Chan et al. in [27], to study the mathematical properties of variational image inpainting. This model can be applied to the image when using the level sets of an image. The formula of the Euler-Elastic model can be introduced as follows:

$$\boldsymbol{E(u,\Gamma) = \min_{u}\int_{\Gamma}(\alpha + \beta k^2) ds} \quad (3.14)$$

where α and β are control parameters, k is the curvature, ds the length element. After that, the Euler-Lagrange Equation is applied on (3.14), which produces a 2nd-order PDE. Euler-Elastica model is used to rebuild the destroyed regions based on linking T-crosses at the boundaries of the area [4]. The minimization of a bounded Euler elastic energy is applied to expand the idea of the length of curvature from the edges to all the level lines of the image [35].

3.6.Mumford-Shah-Euler Model (MESM)

The MESm was introduced to overwhelmed the flaws of the MSm by developing its curve model [25]. The MESm formula is:

$$\boldsymbol{E(u,\Gamma) = \min_{u} F(u,\Gamma) = \frac{\lambda}{2}\int_{\Omega\setminus D}(u-f)^2\, d\vec{x} + J(u,\Gamma)} \quad (3.15)$$

with

$$\boldsymbol{J(u,\Gamma) = \frac{\gamma}{2}\int_{\Omega\setminus\Gamma}|\nabla u|^2 d\vec{x} + \int_{\Gamma}(\alpha + \beta k^2) ds} \quad (3.16)$$

The formula (3.15) denotes the MSm, while the formula (3.16) is the Euler-Elastica method, which is introduced based on studying the mechanical properties of a thin and sprain-free rod [39]. After that, the Euler-Lagrange Equation is applied on (3.16), which produces a 4th-order PDE. The same numerical technique that applied for solving MSm will be followed to solve MSEm.

This model successfully reconstructed the small textured damaged areas in the images [25]. In summary, this model succeeded to achieve the connectivity principle and the curvature preservation

through reconstructing large damaged areas in the non-textured images. While this model never successfully recovered the big textured damaged areas in the images.

3.7.Modified Chan-Hilliard Model (mCH)

The mCH model is introduced for binary image inpainting [26], this model also applies in material sciences [40]. The formula of mCH model is:

$$\boldsymbol{\partial_t u} = \Delta\left(-\boldsymbol{\epsilon}\Delta\boldsymbol{u} - \frac{\mathbf{1}}{\boldsymbol{\epsilon}}\boldsymbol{F'(u)}\right) + \boldsymbol{\lambda}\,(\vec{\boldsymbol{x}})(\boldsymbol{f}-\boldsymbol{u}),\ \ \boldsymbol{in\Omega} \qquad (\mathbf{3.17})$$

Where $$\boldsymbol{\lambda}(\vec{\boldsymbol{x}}) = \begin{cases} \mathbf{0} & \boldsymbol{if}\ \vec{\boldsymbol{x}} \in \boldsymbol{D} \\ \boldsymbol{\lambda_0} & \boldsymbol{if}\ \vec{\boldsymbol{x}} \in \boldsymbol{\Omega}\backslash\boldsymbol{D} \end{cases}$$

Where $\boldsymbol{\Omega}$ is image domain, $\boldsymbol{D} \subset \boldsymbol{\Omega}$ is that the inpainting domain, $\boldsymbol{F(u)}$ is denotes a double-well potential, and $\boldsymbol{F(u)} = \left(\mathbf{1} - \boldsymbol{u^2}\right)^{\mathbf{2}}/\mathbf{4}$, where $\boldsymbol{\epsilon}$ is a positive constant that tends to zero. The model (3.17) is a semi-linear 4th-order PDE. To solve model ($\boldsymbol{3}$.17), enough solution the functional formula ($\boldsymbol{3}$.18):

$$\int_{\boldsymbol{\Omega}} \frac{\boldsymbol{\epsilon}}{\mathbf{2}}|\boldsymbol{\nabla u}|^2 + \frac{\mathbf{1}}{\boldsymbol{\epsilon}}\boldsymbol{F(u)}\boldsymbol{d\vec{x}} + \boldsymbol{\lambda_0}\int_{\boldsymbol{\Omega\backslash D}} (\boldsymbol{f}-\boldsymbol{u})^2\,\boldsymbol{d\vec{x}} \qquad (\mathbf{3.18})$$

The convexity splitting method applied on (3.18), this splitting produces a 4th-order PDE. The numerical method used to solve this model can be found in [26]. This model succeeded in reconstructing large damaged areas in a visually acceptable way [26].

4. PDE-BI Methods

A PDE- based inpainting method was firstly introduced by Bertalmio et al. in [1]. The user only locates the regions to be recovered, then the application automatically reconstructed them. A PDE-based image inpainting problem studied various from a PDE-based image denoising problem because the noise parts of the images include both real data and the noise information, while the damaged regions include no information at all in image inpainting. PDE-BI models are directly defined by PDE as follows:

$$\boldsymbol{\partial_t u} = \boldsymbol{F}\left(\boldsymbol{x}, \boldsymbol{u}, \boldsymbol{Du}, \ldots, \boldsymbol{D^k u}\right),$$

where $\boldsymbol{F}: \boldsymbol{\Omega} \times \mathbb{R} \times \mathbb{R}^{\mathbf{2}} \times \mathbb{R}^{\mathbf{3}} \times \ldots \mathbb{R}^{\boldsymbol{k}} \rightarrow \mathbb{R}$ denotes a kth-order differential operator. Examples of PDE-BI models that have been introduced in the literature include the isotropic diffusion [17], Transport [1], Navier Stokes [19], and Harmonic [18]. Next, a review of some different PDE-BI methods will introduce.

4.1. Isotropic Diffusion (Tikhonov Regularisation Method)

The isotropic model was firstly introduced for image inpainting [17]. Also, this model has been proposed to reconstruct blurred images [41], [42], and [43]. Image inpainting is analogized with a heat transfer in terms of work procedures. Where the isotropic method works based on spreading the information from the exterior (known pixels) to the interior of damaged regions. The isotropic model is used for recovering damaged regions in the image being corresponding to a temperature domain with the pixel value equivalent to the temperature value. Therefore, pixels values are changed in the missing region as the temperature difference because of the external heat sources resulting from using the heat conduction equation. The formula of the heat equations [44, 45] introduced as follows:

$$\begin{cases} \partial_t u = \Delta u, \quad t \geq 0, \\ u(0, x, y) = 0. \end{cases} \tag{4.1}$$

Also, the formula of the heat equation can be introduced as the minimization energy functional, as follows:

$$\min_{u \in L^2(\Omega)} \left\{ \int \int_D |\nabla u|^2 \, dxdy \quad such\ that \quad u = f \ \ in\ \Omega \backslash D \right\} \tag{4.2}$$

The Euler-Lagrange equation with the gradient descent method has been applied to minimization functional (4.2):

$$u_t = \Delta u \tag{4.3}$$

The finite difference method is applied to solve equation (4.3) which aims to recover the damaged regions in the image. This numerical method will be applied at each pixel of damaged regions in three channels (R, G, B) of the image to reconstruct them. The numerical solutions of this model may fail to recover edges, curvature, and corners. This model needs fewer iteration steps for recovering the damaged regions and it has a faster processing speed. Finally, the curvature preservation and the connectivity principle are not achieved for reconstructing small damaged areas.

4.2. Harmonic Extension Model

The harmonic model is introduced as a simple example to understand the image interpolation process. The damaged regions can be recovered by the numerical solutions of the Laplace equation, or by the numerical solutions of the energy minimization over the inpainting domain. This model can be defined as the minimizer of energy [18], as follows:

$$\min_{u \in L^2(\Omega)} \int \int_{\Omega} \left(|\nabla u|^2 + \lambda |u - f|^2_{L^2(\Omega)} \right) dxdy = 0, \quad in\ D, \qquad u = f \ \ on \partial\, D, \tag{4.4}$$

where $\boldsymbol{\lambda}$ is a constant parameter. The Euler-Lagrange equation is applied on (4.4), as follows:

$$\begin{cases} -\Delta u = 0, & in\ D, \\ -\Delta u = \lambda (f - u), & in\ \Omega \backslash D, \\ u = 0, & on\ \partial\Omega. \end{cases} \tag{4.5}$$

The harmonic model succeeded to smoothly reconstruct the small damaged areas. Nevertheless, the harmonic model failed to recover the edges and large damaged areas. Finally, the connectivity principle is achieved through recovering small damaged areas, but the curvature preservation is not achieved.

4.3. Navier-Stokes Equation

The image inpainting problem has been introduced by Bertozzi et al in [19] based on the ideas from computational fluid dynamics. Where the correspondence between concepts of fluid dynamics and variational inpainting is found. Navier-Stokes equation is one of fluid dynamics equations. Navier-Stokes method is the DEs that control the behavior of the Newtonian incompressible fluid by conjugation the compression and speed field of a fluid. Thus, the parallel exploitation between 2-dim incompressible fluid stream and image intensity function to evolving a different inpainting method.

For this inpainting problem, the intensity image is represented as the flow function. The smoothness image is obtained by applying the Laplacian operator on the image. Isophote operator is a line direction that represents the direction of flow fluid lines, and the anisotropic diffusion matches for fluid viscosity. In this inpainting operation, the discrete lines or curvatures are linked by isophotes, while gradient vectors are matching at the boundary of the unknown region. The formula of the Navier-Stokes equation for image inpainting is:

$$\boldsymbol{w_t + v \cdot \nabla w = V\nabla \cdot (g(|\nabla w|)\nabla w)}, \qquad (\mathbf{4.6})$$

where $\Delta \boldsymbol{I} = \boldsymbol{w}$ is the vorticity, and $\boldsymbol{\nabla^{\perp} I = v}$ denotes the perpendicular gradient. In this implementation, the user only locates the damaged regions. then, these regions are automatically filled. The diffusion is large for smooth areas while it is close to zero on edges ([5]). There are several efficacy convergent numerical methods prepared to solve them. The solution quality of these equations is not better than the quality of the solutions obtained by transport equation [1], but the computations time is developed from few minutes to few seconds.

4.4.Transport Method (Bertalmio)

PDE-BI methods are introduced based on transport dynamics [1], paved the way for the modern PDE-BI method. The transport model has been proposed based on the idea of manual inpainting into a mathematical and algorithmic language. The formula of the transport model is:

$$\boldsymbol{\delta u^n \cdot u_t^n = 0}, \qquad (\mathbf{4.7})$$

where $\mathbf{\delta u^n}$ is projected propagation direction, and $\boldsymbol{u_t^n}$ denotes smoothing information propagation. This algorithm is an iterative operation spreading linear geometry (edges) into the damaged area from the surrounding areas. The diffusion operation is introduced as follows:

$$\boldsymbol{u^{n+1}(i,j) = u^n(i,j) + \Delta t \cdot u_t^n(i,j), \quad \forall (i,j) \in \Omega} \qquad (4.8)$$

The Laplacian operator is applied to produce a smooth image. The vertical direction to the gradient multiplies in the Laplacian operator. The transport method formula is

$$\boldsymbol{u_t^n = \nabla(\Delta u) \cdot \nabla^{\perp} u} \qquad (4.9)$$

Where $\Delta \boldsymbol{t}$ is the isophotes direction ($\Delta \boldsymbol{t}$) is the Laplacian smoothness operation on the gradient.

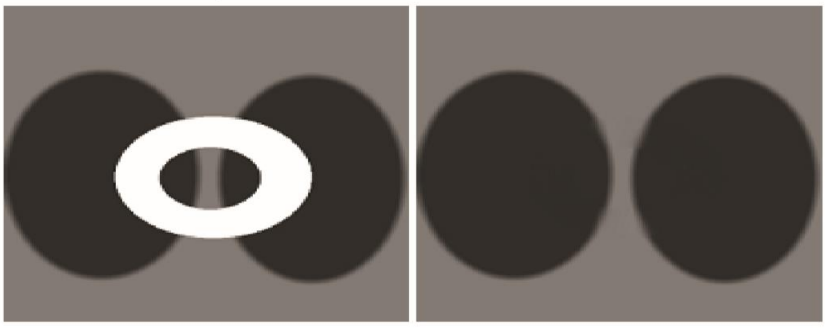

Figure 2. (a) Destroyed image (b) Inpainted image is taken from [1].

The main drawbacks of this model are its weak performance in the reconstruction of big textured areas because produced blurring artefacts by the propagation process and the shortage of explicit handling of

the pixels on the edges. Finally, both the connectivity principle and the curvature preservation are not achieved to reconstruct the big damaged areas. While this model successfully recovered the curvature, edges, and corners in the small damaged areas.

5. Comparison of PDE-BI and Variational methods.

A summarizes the above approaches providing additional knowledge about the positive aspects and limitations of each approach. Table 1 shows the comparison among the different Variational and PDE-BI methods used for the inpainting.

Table 1. Comparison of various PDE-BI and variational methods.

No.	PDE-BI method	Merits	Demerits
1	Heat transfer	It produces good results if missing regions are small ones.	It takes a long time and does not well if missing regions are large.
2	Harmonic	Fast and simple	Produced blurred results when the destroyed regions are large.
3	Navier-Stokes	Stability and speed are improved. It produces well results for non-textured small damaged areas.	Requires user interactions, produces blurred results. It takes a long time for the large target area.
4	Mumford-Shah	Works well and fast for small regions.	Produced blurred results when the missing regions are large and edges need to be propagated.
5	Mumford-Shah-Euler	Approximation and computations are decreased.	Produced artifacts corner, violates connectivity, not stable.
6	Modified Chan-Hilliard	Works well for recovering large destroyed regions, and its successes to preserve the edges.	Produces artifacts when the surrounding areas of the destroyed region are the texture.
7	Bertalmio (Transport)	Performs well for small non-texture region and noise removal application.	The process of this method produces blurring when applying for large damaged areas and high texture areas surrounding it.
8	Total Variation	Works well for removing salt and pepper noise. And recovers small non-texture regions.	Models recovering only small miniature regions.
9	High order Total Variation	Produces well results near the boundary. Also, it is fast.	Producing artifacts for recovering large textured damaged areas, it depends on parameter tuning.
10	Curvature of Driven Diffusion (CDD)	Used for bigger non-textured areas and connect some simply broken edges.	Results look blurred for large broken edges and time-consuming.
11	Euler-Elastica	Used for small non-texture missing regions.	Produces artifacts when the region is a texture or large.

6. Conclusion and Future Works

This survey paper presents several inpainting methods such as PDE-BI and variational-BI local methods. Four PDE-BI methods have been studied such as Transport, Navier-stokes, Harmonic-

Extension, and Isotropic Diffusion equations. Seven Variational-BI models have been studied such as Mumford-Shah, TV, CDD, High order TV, Mumford-Shah-Euler, Chan-Hilliard, and Euler-Elastica and curvature.

Also, a comparative study of PDE-BI and variational-BI methods have been introduced to evaluate the performance of these methods and to clarify the benefits and drawbacks for each one of them. Although many PDE-IB methods are suggested in the last years, however, it remains difficult to determine the best one. The 4th-order PDE methods are succeeded in recovering edges and corners such as MESm, mCH, and 4th order TV.

The 2nd-order PDE methods are succeeded in reconstructing small destroyed areas however they failed to recover the edges and corners such as TV, Harmonic, isotropic, anisotropic, Euler-Elastica, and MS methods. Therefore, the 4th-order PDE methods were succeeded to defeat the restrictions intrinsic to 2nd-order PDEs. To conclude, we conclude the high-order PDE-BI and variational-IB methods outperform 2nd-order PDE-BI and variational-IB methods in reconstructing small destroyed areas in an image. Nevertheless, all of these methods have restrictions when they recovered large destroyed areas with high texture in the surrounding areas.

Therefore, to overcome these problems, we need a powerful method to reconstruct both small and large areas in a small computational time. So, we will propose a PDE-IB method based on using the non-linear diffusion tensor to recovers the destroyed regions and preserves discontinuities. Also, the extended wavelet transform can be used to enhance the edges. Moreover, we are also currently working on the combination of three inpainting methods to reconstructing large destroyed texture regions in the images which are called hybrid inpainting technique.

TDA approach proposed to assess the quality of natural denoised images and to study the efficacy of PDE-based denoised models. More accurately, the number of CCs is counted for both the denoised and original images. The closer number of CCs of the denoised image to the number of CCs of the original image is the better quality of the denoised image and consequently is the better denoising model. Experimental results showed the efficacies of the TV-L^1 and 4^{th}-order model for removing the noise are better than the TV-L^2 model, and the efficacies of the 4^{th}-order model in edge preservation are better than TV-L^1 and TV-L^2 models. Also, the TV-L^1 and TV-L^2 models needed a large number of iterations to arrive in the steady-state however they are still faster than in the 4^{th} -order model. The TDA approach gave a good evaluation of image denoising quality because their results corresponding with their qualitative results. In the future, the image quality will study and analysis under other types of noise and denoising models.

References

[1] M Bertalmio, G. Sapiro, V Caselles, and C Ballester 2000 Image inpainting *Proc. 27th Annu. Conf. Comput. Graph Interact Tech (SIGGRAPH 00*, vol 2) no 5 pp 417–424.
[2] T F Chan, and J Shen 2002 Mathematical models for local nontexture inpaintings, *SIAM Journal on Applied Mathematics* vol 62 (Society for Industrial and Applied Mathematics) pp 1019–1043.
[3] V Caselles, J M Morel, and C Sbert 1999 An axiomatic approach to image interpolation.
[4] T Nitzberg, M Mumford, and D Shiota 1993 Filtering, Segmentation, and Depth, (Berlin: Springer-Verlag).
[5] S Masnou, and J M Morel 1998 Level lines based disocclusion, in *Proceedings 1998 International Conference on Image Processing, ICIP98* (Cat. No.98CB36269) vol 3 pp 259–263.

[6] T F Chan, and J (Jackie) Shen 2005 Variational image inpainting, *Commun. Pure Appl. Math.*, vol 58 no 5 pp 579–619.
[7] L I Rudin, S Osher, and E Fatemi 1992, Nonlinear total variation based noise removal algorithms (*Phys. D Nonlinear Phenom)* vol 60 no 1–4 pp 259–268.
[8] A Criminisi, P Perez, and K Toyama 2004 Region filling and object removal by exemplar-based image inpainting *IEEE Trans. Image Process.* vol 13 no 9 pp 1200–1212.
[9] W H Cheng, C W Hsieh, S K Lin, C W Wang, and J L Wu 2005 Robust algorithm for exemplar-based image inpainting *Process Int. Conf. Comput. Graph.* pp 64–69.
[10] S A Jassim, A K Al-jaberi, A T Asaad, and N Al-Jawad 2018 Topological data analysis to improve exemplar-based inpainting *Mobile Multimedia/Image Processing, Security, and Applications 2018*, vol 10668 p 4.
[11] K Sangeeth, P Sengottuvelan, and E Balamurugan 2011 A novel exemplar based Image Inpainting algorithm for natural scene image completion with improved patch prioritizing *Int. J. Comput. Appl.* vol 36 no 4 pp 0975–8887.
[12] Jiying Wu, and Qiuqi Ruan 2008 A novel hybrid image inpainting model *2008 International Conference on Audio, Language and Image Processing*, pp 138–142.
[13] M Bertalmio, L Vese, G Sapiro, and S Osher 2003 Simultaneous structure and texture image inpainting *IEEE. Trans. Image Process.* vol 12 no 8 pp 882–889.
[14] T Kim, and L Cai 2015 Context-driven hybrid image inpainting *IET. Image Process.* vol 9 no 10 pp 866–873.
[15] A A Efros, and T K Leung 1999 Texture synthesis by non-parametric sampling *Proceedings of the Seventh IEEE International Conference on Computer Vision* vol 2 pp 1033–1038.
[16] L Y Wei, and M Levoy 2000 Fast Texture Synthesis using Tree-structured Vector Quantization (*Proc 27th Annu Conf Comput Graph Interact Tech)*, vol ACM Press, pp 479–488.
[17] G Aubert, and P Kornprobst 2006 Mathematical problems in image processing : partial differential equations and the calculus of variations (Springer).
[18] J Shen, and T F Chan 2002 Mathematical models for local nontexture inpaintings *SIAM. J. Appl. Math.* vol 62 no 3 pp 1019–1043.
[19] M. Bertalmio, A L Bertozzi, and G Sapiro 2001 Navier-Stokes, fluid dynamics, and image and video inpainting.
[20] G. Emile-Mâle 1976 The restorer's handbook of easel painting (*Van Nostrand Reinhold)*.
[21] S Walden 1985 The ravished image: or how to ruin masterpieces by restoration *Weidenfeld. and Nicholson. St. Martins*.
[22] T C, and J Shen 2001 Local inpainting models and TV inpainting *SIAM. J. Appl. Math.* vol 62 no 3 pp 1019–1043.
[23] T Chan, and J.Shen 2001 Non-texture inpainting by Curvature-Driven Diffusions (CCD) *J. V. is Commun Image Represent.* vol 12(4) pp 436–449.
[24] M Burger, L He, and C B Schönlieb 2009 Cahn–Hilliard inpainting and a generalization for grayvalue images *SIAM. J. Imaging Sci.* vol 2 no 4 pp 1129–1167.
[25] E S, and S Jianhong 2002 Digital Inpainting Based On The Mumford-Shah-Euler Image Model *Eur. J. Appl. Math.* vol 4 pp 353–370.
[26] A L Bertozzi, S Esedoglu, and A Gillette 2007 Inpainting of binary images using the Cahn–Hilliard equation *IEEE. Trans. Image Process.* vol 16 no 1 pp 285–291.
[27] T F Shen, J Kang, S H, and Chan 2002 Euler's elastica and curvature-based inpainting *SIAM. J. Appl. Math.* vol 63 pp 564–592.
[28] C B Schönlieb, A Bertozzi, M Burger, and L He 2010 Image inpainting using a fourth-order total variation flow *SAMPTA'09*, p Special session on sampling and inpainting.
[29] A K Al-jaberi, N Al-jawad, and S A Jassim 2018 Colourizing monochrome images *Mobile*

Multimedia/Image Processing, Security, and Applications 2018 vol 10668 p 5.
[30] G W Recktenwald 2004 Finite-difference approximations to the heat equation.
[31] Wei Guo, and Li-Hong Qiao 2007 Inpainting based on total variation *2007 International Conference on Wavelet Analysis and Pattern Recognition* pp 939–943.
[32] T F Chan, and J Shen 2001 Nontexture inpainting by Curvature-Driven Diffusions *J. V. is Commun Image Represent*, vol 12 no 4 pp 436–449.
[33] T F Chan, J Shen, and H M Zhou 2006 Total variation wavelet inpainting *J. Math. Imaging V.* vol 25.1 pp 107–125.
[34] A Tavakoli, P Mousavi, and F Zarmehi 2018 Modified algorithms for image inpainting in Fourier transform domain *Comput. Appl. Math.* vol 37 no 4 pp 5239–5252.
[35] D Mumford 1994 Elastica and computer vision *Algebraic Geometry and its Applications* New York, NY: Springer New York pp 491–506.
[36] C B Schönlieb 2009 Modern PDE techniques for image inpainting, (*Dr Diss Univ Cambridge)*.
[37] A Tsai, A Yezzi, and A S Willsky 2001 Curve evolution implementation of the Mumford–Shah functional for image segmentation denoising, interpolation, and magnification *IEEE. Trans. IMAGE Process.* vol 10 no 8 pp 1169–1186.
[38] C B Schonlieb 2015 Partial differential equation methods for image inpainting (*Cambridge: Cambridge University Press)*.
[39] A E H Love 2013 A treatise on the mathematical theory of elasticity *(London: Cambridge University Press)*.
[40] J W Cahn, and J E Hilliard 1958 Free energy of a nonuniform system I. Interfacial Free Energy, *J. Chem. Phys.* vol 28 no 2 pp 258–267.
[41] J Weickert 1998 Anisotropic Diffusion in Image Processing Vol 1.
[42] J Weickert, 1996, Theoretical foundations of anisotropic diffusion in image processing.
[43] C Guillemot, and O Le Meur 2014 Image inpainting : Overview and recent advances *IEEE. Signal Process. Mag*.
[44] A Robles-Kelly, and E R Hancock 2004 Vector field smoothing via heat flow.
[45] Shubham Sharma and Ahmed J. Obaid 2020 J. Phys.: Conf. Ser. 1530 012124

Acknowledgments
We thank applied school in university of Buckingham, for providing the lab to work in it. We also thank college of education for pure science in university of Basrah for encouraging our to finish this work.